5 Modeling Voltage-Dependent Channels

Alain Destexhe and John R. Huguenard

5.1 Introduction

Many different types of voltage-dependent ion channels have been identified and are responsible for a rich repertoire of electrical behavior essential for neuronal function (Llinás, 1988). Modeling voltage-dependent ion channels is crucial for assessing their numerous roles in the genesis of the complex intrinsic properties of central neurons, as well as how such neurons integrate synaptic inputs with intrinsic excitability to generate spike output. The seminal work of Hodgkin, Huxley, Katz, and others several decades ago still constitutes the basis of today's models. The first accurate model of membrane excitability was introduced by Hodgkin and Huxley (1952) and was based on relatively simple biophysical mechanisms underlying the Na^+ and K^+ conductances that generate action potentials in the giant axon of the squid. This model reproduced well the behavior of the recorded currents, and its parameters are easy to determine from experimental data. This explains why Hodgkin-Huxley models are still widely used today, almost sixty years later.

The postulate of the Hodgkin-Huxley model was that membrane currents result from the assembly of gating particles freely moving in the membrane. The molecular components responsible for ionic permeabilities were later identified as being transmembrane protein complexes containing a pore specifically permeable to one or several ions (reviewed in Hille, 2001). These ion channels can have their permeability modulated by various factors, such as the voltage or the binding of a ligand. The sensitivity of some ion channels to voltage is a fundamental property that constitutes the core mechanism underlying the electrical excitability of membranes and is still today an important matter of investigation (for a review, see Armstrong and Hille, 1998). In particular, the Hodgkin-Huxley model was cast in a formalism more compatible with statistical physics and thermodynamics (Tsien and Noble, 1969; T. L. Hill and Chen, 1972; Stevens, 1978), which we call here thermodynamic models.

Single-channel recording techniques (reviewed in Sakmann and Neher, 1995) provided significant advances in our understanding of the biophysical properties of ion

channels. Single-channel recordings have shown that ion channels display rapid and stochastic transitions between conducting and nonconducting states. It is now known that conformational changes of the channel protein give rise to opening and closing of the channel. Conformational changes in ion channels can be described by state diagrams analogous to the conformational changes underlying the action of enzymes (chapter 3, section 2). Markov models are based on such transition diagrams and have been used for modeling various types of ionic currents based on single-channel recordings (for a complete overview, see Sakmann and Neher, 1995). This formalism is more accurate than Hodgkin-Huxley models, but its drawback is the greater difficulty of estimating its parameters from experimental data (Cannon and D'Alessandro, 2006). However, Markov models can also be used to draw simplified representations of the current, which capture only the most salient properties of voltage-dependent or synaptic interactions (Destexhe et al., 1994). Such simplified models are more adequate for representing currents when simulating networks involving thousands of cells.

Thus, various formalisms of different levels of complexity have been proposed to model ionic currents. Which formalism to adopt for modeling a given current depends on the experimental data available and its accuracy, as well as the desired level of precision in the behavior of the model. We illustrate these aspects in this chapter by considering different types of formalisms in modeling such processes as the action potential and voltage-clamp recordings of the T-type calcium current in thalamic neurons. For both cases, we show the similarities and differences among the different models, how well they account for experimental data, and which is the "minimal" model needed to reproduce electrophysiological behavior.

5.2 The Hodgkin-Huxley Formalism

The Hodgkin-Huxley Model

In a remarkable series of experiments on the squid giant axon, Hodgkin, Huxley, and colleagues determined that ionic conductances can be activated or inactivated according to the membrane potential. They used the technique of a voltage clamp to record the ionic currents generated at different voltages and thus infer how these currents can be dynamically modulated by voltage. They characterized the kinetics of two voltage-dependent currents, the fast sodium current, I_{Na}, and the delayed potassium rectifier, I_K, mediated by Na^+ and K^+ ions, respectively. A mathematical model was necessary to establish that the identified kinetic properties of voltage dependence were sufficient to explain the genesis of action potentials. The model introduced by Hodgkin and Huxley (1952) incorporated the results of their voltage-clamp

experiments and successfully accounted for the main properties of action potentials, which represented very convincing evidence that their postulated mechanism was plausible.

The Hodgkin-Huxley model is based on a membrane equation describing three ionic currents in an isopotential compartment:

$$c_m \frac{dV}{dt} = -g_L(V - E_L) - g_{Na}(V)(V - E_{Na}) - g_K(V)(V - E_K), \tag{5.1}$$

where c_m is the membrane capacitance; V is the membrane potential; g_L, g_{Na}, and g_K are the membrane conductances for leak currents, Na^+, and K^+ currents respectively; and E_L, E_{Na}, and E_K are their respective reversal potentials, which are given by the Nernst relation (equation 5.11).

The critical step in the Hodgkin-Huxley model is to specify how the conductances $g_{Na}(V)$ and $g_K(V)$ depend on the membrane potential V. Hodgkin and Huxley hypothesized that ionic currents result from the assembly of several independent gating particles that must occupy a given position in the membrane to allow the flow of Na^+ or K^+ ions (Hodgkin and Huxley, 1952). Each gating particle can be on either side of the membrane and bears a net electronic charge such that the membrane potential can switch its position from the inside to the outside or vice versa. The transition from these two states is therefore voltage dependent, according to the diagram:

$$\text{(outside)} \underset{\beta_m(V)}{\overset{\alpha_m(V)}{\rightleftharpoons}} \text{(inside)}, \tag{5.2}$$

where α and β are, respectively, the forward and backward rate constants for the transitions from the outside to the inside position in the membrane. If m is defined as the fraction of particles in the inside position, and $(1 - m)$ as the fraction outside, one obtains the first-order kinetic equation:

$$\frac{dm}{dt} = \alpha_m(V)(1 - m) - \beta_m(V)m. \tag{5.3}$$

Assuming that particles must occupy the inside position to conduct ions, then the conductance must be proportional to some function of m. In the case of the squid giant axon, Hodgkin and Huxley (1952) found that the nonlinear behavior of the Na^+ and K^+ currents, their delayed activation, and their sigmoidal rising phase were best fit by assuming that the conductance is proportional to the product of several of such variables:

$$g_{Na} = \bar{g}_{Na} m^3 h \tag{5.4}$$

$$g_K = \bar{g}_K n^4, \tag{5.5}$$

where $\bar{g}_{Na}$ and $\bar{g}_K$ are the maximal values of the conductances, while m, h, and n represent the fraction of three different types of gating particles in the inside of the membrane. This equation allowed them to accurately fit the voltage-clamp data of the currents. Their interpretation is that the assembly of three gating particles of type m and one of type h is required for Na^+ ions to flow through the membrane, while the assembly of four gating particles of type n is necessary for the flow of K^+ ions. These particles operate independently of each other, leading to the m^3h, and n^4 forms.

Long after the work of Hodgkin and Huxley, when it was established that ionic currents are mediated by the opening and closing of ion channels, the gating particles were reinterpreted as *gates* inside the pore of the channel. Thus, the reinterpretation of Hodgkin and Huxley's hypothesis was that the pore of the channel is controlled by four internal gates, that these gates operate independently of each other, and that all four gates must be open in order for the channel to conduct ions.

The rate constants $\alpha(V)$ and $\beta(V)$ of m and n are such that depolarization promotes opening the gate, a process called *activation*. On the other hand, the rate constants of h are such that depolarization promotes closing of the gate (and therefore closing of the entire channel because all gates must be open for the channel to conduct ions), a process called *inactivation*. Thus the experiments of Hodgkin and Huxley established that three identical activation gates (m^3) and a single inactivation gate (h) are sufficient to explain the Na^+ current's characteristics. The squid axon K^+ current does not have inactivation and can be well described by four identical activation gates (n^4).

Taking together all the steps here, one can write the following set of differential equations, called Hodgkin-Huxley equations (Hodgkin and Huxley, 1952):

$$\begin{aligned}
C_m \frac{dV}{dt} &= -g_L(V - E_L) - \bar{g}_{Na} m^3 h (V - E_{Na}) - \bar{g}_K n^4 (V - E_K) \\
\frac{dm}{dt} &= \alpha_m(V)(1 - m) - \beta_m(V) m \\
\frac{dh}{dt} &= \alpha_h(V)(1 - h) - \beta_h(V) h \\
\frac{dn}{dt} &= \alpha_n(V)(1 - n) - \beta n(V) n.
\end{aligned} \tag{5.6}$$

Hodgkin and Huxley (1952) estimated the rate constants (α_i and β_i) by fitting empirical functions of voltage to the experimental data. These functions are

$$\begin{aligned}
\alpha_m &= \frac{-0.1(V - V_r - 25)}{\exp[-(V - V_r - 25)/4] - 1} \\
\beta_m &= 4 \exp[-(V - V_r)/18] \\
\alpha_h &= 0.07 \exp[-(V - V_r)/20] \\
\beta_h &= \frac{1}{1 + \exp[-(V - V_r + 30)/10]} \\
\alpha_n &= \frac{-0.01(V - V_r + 10)}{\exp[-(V - V_r + 10)/10] - 1} \\
\beta_n &= 0.125 \exp[-(V - V_r)/80].
\end{aligned} \tag{5.7}$$

These functions were estimated at a temperature of 6 °C (see section 5.7 for temperature dependence) and the voltage axis has been reversed in polarity (voltage values were given with respect to the resting membrane potential, V_r) compared to the original study.

The Hodgkin-Huxley model is often written in a form more convenient to fit to experimental data by rewriting equation (5.3) in the equivalent form:

$$\frac{dm}{dt} = \frac{1}{\tau_m(V)}[m_\infty(V) - m], \tag{5.8}$$

where

$$m_\infty(V) = \alpha(V)/[\alpha(V) + \beta(V)] \tag{5.9}$$

$$\tau_m(V) = 1/[\alpha(V) + \beta(V)]. \tag{5.10}$$

Here, m_∞ is the *steady-state activation* and τ_m is the *activation time constant* of the Na^+ current (n_∞ and τ_n represent the same quantities for the K^+ current). In the case of h, h_∞ and τ_h are called steady-state inactivation and inactivation time constant, respectively. These quantities are important because they can easily be determined from voltage-clamp experiments. The Boltzmann equation (Hille, 2001; equation 2.1) is commonly used for for $m_\infty(V)$.

Fitting to Voltage-Clamp Data

We now turn to the problem of how to use the results of voltage-clamp experiments to build a Hodgkin-Huxley type of model. We discuss these protocols and illustrate them for another type of current, the low-threshold calcium current, also called the T-type calcium current, T-current, or I_T. To this end, we use data collected

previously (Huguenard and Prince, 1992) using whole-cell patch recordings from acutely dissociated thalamic relay neurons from the ventrobasal thalamus of young rats (P8–P15). All recordings correspond to a temperature of 24 °C (see Huguenard and Prince, 1992 for details about those experiments).

Activation

Like Hodgkin-Huxley's Na^+ current, the T-current is transient and activates upon depolarization, but is slower and its voltage range for activation and inactivation typically occurs around resting membrane potential. To reveal activation properties, the typical voltage-clamp protocol is to clamp the membrane using a series of voltage steps from a hyperpolarized level (−100 mV) to various depolarized levels. Such a protocol reveals an inward current that activates and inactivates in a voltage-dependent manner (figure 5.1a2); i.e., each process becomes faster with stronger depolarizations.

Deactivation

Interrupting the activation protocol before inactivation is complete generates tail currents (figure 5.1a1) that reveal the deactivation characteristics of the current. Deactivation is the reversal of the activation process: the m gating particles revert to a closed state during membrane hyperpolarization. Because inactivation is relatively slow (see next), the kinetics of tail currents, which reflect channel closing, at hyperpolarized membrane potentials are predominately dependent on deactivation, which is much faster. Deactivation time constants obtained from tail current analysis are plotted on the left side (i.e., between membrane potentials of −120 to −80 mV) of the bell-shaped curve in figure 5.1c.

Inactivation

The typical voltage-clamp protocol to reveal steady-state inactivation is to apply a series of holding potentials for a prolonged period (several seconds) to allow inactivation to obtain steady-state equilibrium. Then a command potential is applied that activates the current (at −30 mV in this case). This protocol is shown in figure 5.2a1 for the T-current. The different current traces obtained contain similar activation but different levels of inactivation.

Deinactivation

By analogy to deactivation, deinactivation represents the reversal of the inactivation process: h particles revert to an open state during membrane hyperpolarization. The kinetics of deinactivation can be measured by reactivating the current following complete inactivation. This is accomplished by first holding the membrane potential at a depolarized level (−40 mV here) to inactivate the current, followed by step voltage-clamp commands to a hyperpolarized value (−90 mV) for variable amounts of time

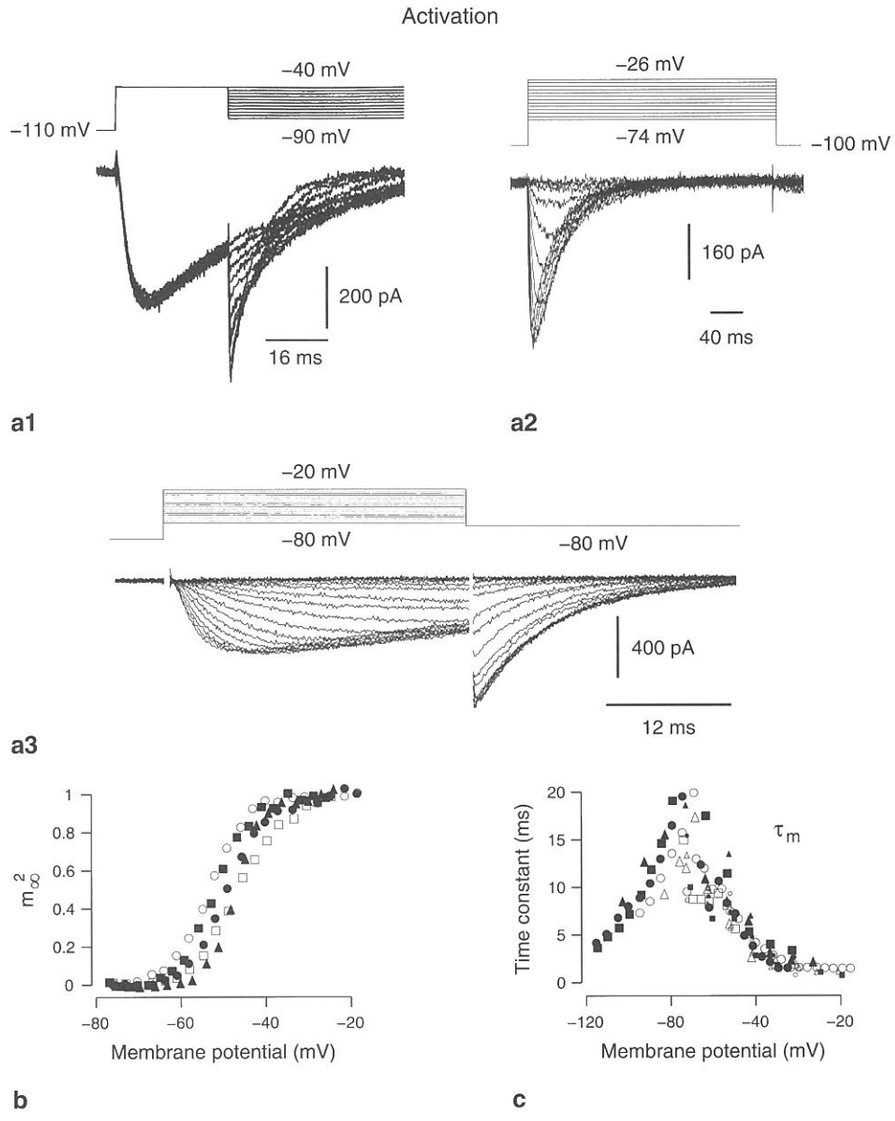

Figure 5.1
Voltage-clamp recordings of the T-current in dissociated thalamic relay neurons. (a) Voltage-clamp protocols for determining deactivation (a1), voltage-dependent activation and inactivation rates (a2), and steady-state activation (a3). Command potentials at various levels were given after the cell was maintained at a hyperpolarized holding potential, leading to the activation of the current. (b) Steady-state activation obtained from the tail currents in a3, which were fit to an m^2h template. (c) Time constants obtained using a similar procedure. Different symbols correspond to different cells. (Figure modified from Huguenard and McCormick, 1992, where all details are given.)

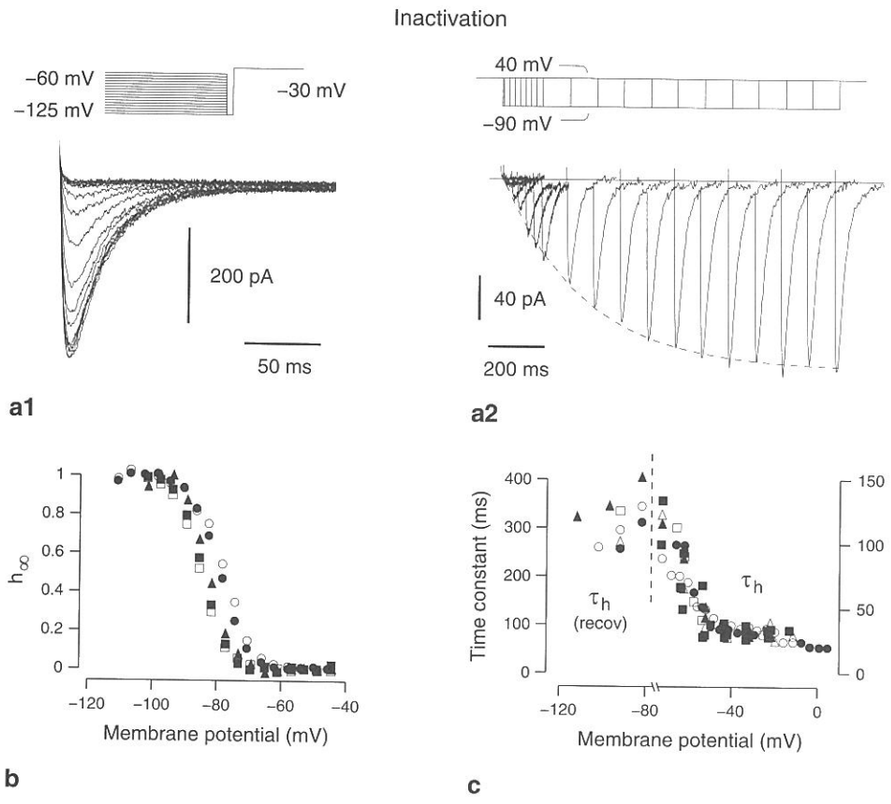

Figure 5.2
Voltage-clamp characterization of T-current inactivation in dissociated thalamic relay neurons. (a) Voltage-clamp protocols for inactivation (a1) and recovery from inactivation (a2). In A1, the cell was maintained at different holding potentials then stepped to −30 mV to activate the T-current with different levels of inactivation. In a2, the current was reactivated after being fully inactivated. The full recovery took about 1 s (recovery time constant of about 300 ms). (b) Steady-state inactivation calculated by the peak of currents in a1. (c) Inactivation time constants obtained by fitting an m^2h template to the data. The recovery time constants were obtained by fitting a single exponential to the recovery experiment (dashed line in a2). Different symbols correspond to different cells. (Figure modified from Huguenard and McCormick, 1992, where all details are given.)

before returning to the initial depolarized level. The second depolarization generates an inward current whose amplitude is proportional to the amount of recovery from inactivation. A particular feature of the T-current is that this recovery from inactivation is very slow (hundreds of millisecond; figure 5.2a2).

Estimating Steady-State Values and Time Constants

Steady-state values and time constants were estimated as follows. First, we assumed that T-current gating could be approximated by the Hodgkin-Huxley formalism for sodium channels, with multiple activation gates and a single inactivation gate (equation 5.4). The optimal number of activation gates was determined by examining differences in residuals between the original current traces and curves best-fitted to various templates (i.e., m^2h, m^3h, and m^4h). This approach originally suggested that m^3h provided the best fit to the data (Coulter et al., 1989). However, later results obtained under conditions that better isolated the T-current (Huguenard and Prince, 1992) proved that the m^2h scheme was more appropriate. Thus the optimal template for the T-current included two activation gates and one inactivation gate (Huguenard and Prince, 1992).

Next, to measure activation, the influence of inactivation must be as minimal as possible. We assumed that activation is essentially complete in 10 ms, and that there is negligible inactivation (these assumptions were checked by calculating the expected activation and inactivation at various voltages). We used the amplitude of the tail current, which reflects the number of channels open at the end of the depolarizing step, as a measure of activation (m^2). The values obtained using this procedure were very close to those obtained by direct fitting of Hodgkin-Huxley equations to current traces (Huguenard and Prince, 1992). The advantage of the tail current approach is that the driving force is the same for all measurements, therefore providing a direct measure of normalized conductance. This type of procedure leads to estimates of steady-state activation (figure 5.1b).

Steady-state inactivation was obtained by plotting the peak current amplitude (obtained at a test potential of −30 mV) as a function of conditioning potential in figure 5.2b). The current traces from which these values were obtained are shown in figure 5.2a1).

The time constants (figures 5.1c and 5.2c) were estimated by fitting the full expression of the current (from equation 5.12) to the current traces (figure 5.1a2), while allowing m and h to evolve as a function of time according to equation (5.3) (see the methods section in Huguenard and McCormick, 1992). Once the steady-state and time constant values are obtained, one must fit either the empirical functions of voltage as done by Hodgkin and Huxley (1952) or by using predefined templates as predicted by theoretical arguments (see section 5.7).

5.3 Implementation

Nernst Equation

In the original Hodgkin-Huxley model, it was assumed that the currents are ohmic, i.e., they vary linearly as a function of voltage and conductance. In such a case, the reversal potential is given by the Nernst equation. For example, for K^+ ions:

$$E_K = \frac{RT}{zF} \ln \frac{[K]_o}{[K]_i}, \tag{5.11}$$

where $R = 8.31\ J \cdot K^{-1} \cdot mol^{-1}$ is the gas constant, T is the absolute temperature in kelvins, z is the valence of the ion ($z = 1$ for K^+ ions, $z = -1$ for Cl^- ions, etc.), $F = 96{,}489\ C \cdot mol^{-1}$ is the Faraday constant, and $[K]_o$ and $[K]_i$ are the concentrations of K^+ ions outside and inside the membrane, respectively (see chapter 3).

Goldman-Hodgkin-Katz Equation

While many ionic currents are ohmic, some show clear deviations from ohmic behavior, which appears as a deviation from linearity in the I–V representation of the current. This deviation, also called *rectification*, may be due to diverse factors, such as very high ionic concentration gradients across the membrane. This is the case for calcium currents in central neurons; the internal and external Ca^{2+} concentrations differ by about four orders of magnitude, and as the ion channels open or close, the membrane never reaches equilibrium (which would be given by the Nernst equation). In such far-from-equilibrium situations, one must use a different formalism. The simplest of such nonlinear models is the *constant-field equation*, also called Goldman-Hodgkin-Katz equation (see details in Hille, 2001). The current is given by

$$I_T = \bar{P}_{Ca} m^2 h G(V, Ca_o, Ca_i), \tag{5.12}$$

where $\bar{P}_{Ca}$ (in centimeters per second) is the maximum permeability of the membrane to Ca^{2+} ions (the permeability here is $\bar{P}_{Ca}\ m^2 h$, the product of maximum permeability and the fraction of channels in an open state), and $G(V, Ca_o, Ca_i)$ is a nonlinear function of voltage and ionic concentrations:

$$G(V, Ca_o, Ca_i) = z^2 F^2 V / RT \frac{Ca_i - Ca_o \exp(-zFV/RT)}{1 - \exp(-zFV/RT)}, \tag{5.13}$$

where $z = 2$ is the valence of calcium ions. Ca_i and Ca_o are the intracellular and extracellular Ca^{2+} concentrations (in molar concentrations), respectively.

5.4 Thermodynamic Models

In the Hodgkin-Huxley model, the rate constants $\alpha(V)$ and $\beta(V)$ were fit to the experimental data by using empirical functions of voltage. An alternative approach is to deduce the exact functional form of the voltage dependence of the rate constants from thermodynamics. These thermodynamic models (Tsien and Noble, 1969; T. L. Hill and Chen, 1972; Stevens, 1978) provide a plausible physical basis for constraining and parameterizing the voltage dependence of rate constants, which are then used to fit voltage-clamp experiments.

In thermodynamic models, the transition between two states of the channel corresponds to a conformational change in the ion channel protein. Consider a transition between an initial (I) and a final (F) state, with a rate constant $r(V)$ that is voltage dependent:

$$I \xrightarrow{r(V)} F. \tag{5.14}$$

According to the theory of reaction rates (Eyring, 1935; F. H. Johnson et al., 1974), the rate of the transition depends exponentially on the free-energy barrier between the two states:

$$r(V) = r_0 e^{-\Delta G(V)/RT}, \tag{5.15}$$

where r_0 is a constant and $\Delta G(V)$ is the free-energy barrier, which can be written as

$$\Delta G(V) = G^*(V) - G_0(V), \tag{5.16}$$

where $G^*(V)$ is the free energy of an intermediate state (activated complex), and $G_0(V)$ is the free energy of the initial state, as illustrated in figure 5.3. The relative values of the free energy of the initial and final states (G_0 and G_1) determine the equilibrium distribution between these states, but the kinetics of the transition depend on the size of the free-energy barrier $\Delta G(V)$. Systems with a smaller energy barrier (figure 5.3, dashed line) correspond to faster kinetics because a larger proportion of molecules will have the energy required to form the activated complex and make the transition.

In ion channels, these different states correspond to different conformations of the ion channel protein. How the transition rates between these conformational states depend on membrane potential is given by the voltage dependence of the free-energy barrier, which is in general difficult to evaluate. The effect of the electrical field on a protein will depend on the number and position of its charged amino acids, which will result in both linear and nonlinear components in the free energy. Without assumptions about the underlying molecular structure, the free energy of a given state i can be written as a Taylor series expansion of the form:

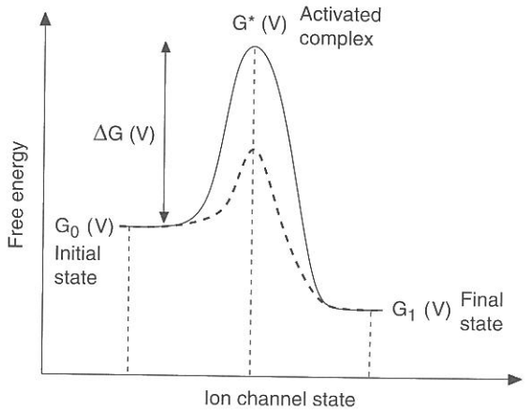

Figure 5.3
Schematic representation of the free-energy profile of conformational changes in ion channels. The diagram represents the free energy of different states involved in a transition: the initial state, activated complex, and final state. The equilibrium distribution between initial and final states depends on the relative value of their free energy (G_0 and G_1). The rate of the transition will be governed by the free-energy barrier ΔG, which is the free-energy difference between the activated complex and the initial state. If the energy barrier is smaller (dashed line), the kinetics of the reaction is faster because a larger proportion of ion channels will have the energy required to make the transition. (Figure modified from Destexhe and Huguenard, 2000.)

$$G_i(V) = A_i + B_i V + C_i V^2 + \cdots \tag{5.17}$$

where $A_i, B_i, C_i, \ldots$ are constants that are specific for each conformational state. The constant A_i corresponds to the free energy that is independent of the electrical field; the linear term $B_i V$ corresponds to the interaction between an electrical field with isolated charges and rigid dipoles (Tsien and Noble, 1969; T. L. Hill and Chen, 1972; Stevens, 1978; Andersen and Koeppe, 1992). For example, linear terms in V will result if the conformations differ in their net number of charges, or if the conformational change is accompanied by the translation of a freely moving charge inside the structure of the channel (T. L. Hill and Chen, 1972; Hille, 2001). Nonlinear terms result from such effects as electronic polarization and pressure induced by V (T. L. Hill and Chen, 1972; Stevens, 1978; Andersen and Koeppe, 1992) or from mechanical constraints associated with the movement of charges that are due to the structure of the ion channel protein (Destexhe and Huguenard, 2000).

Thus, each conformational state of the ion channel protein will be associated with a given distribution of charges and will therefore be characterized by a given set of coefficients in equation (5.17). This is also true for the activated state, which is a particular case of conformation. Applying equations (5.15)–(5.17), the rate constant becomes

$$\begin{aligned} r(V) &= r_0 e^{-[(A^* + B^* V + C^* V^2 + \cdots) - (A_0 + B_0 V + C_0 V^2 + \cdots)]/RT} \\ &= r_0 e^{-(a + bV + cV^2 + \cdots)/RT}, \end{aligned} \tag{5.18}$$

where $a = A^* - A_0, b = B^* - B_0, c = C^* - C_0, \ldots$ represent differences between the linear and nonlinear components of the free energy of the initial and activated states (according to equation 5.17).

Consider the particular case of a reversible open-closed transition

$$C \underset{\beta(V)}{\overset{\alpha(V)}{\rightleftharpoons}} O, \tag{5.19}$$

where C and O are, respectively, the closed and open states, and α and β are the forward and backward rate constants. Applying equation (5.18) to forward and backward reactions leads to the following general expression for the voltage dependence:

$$\begin{aligned} \alpha(V) &= \alpha_0 e^{-(a_1 + b_1 V + c_1 V^2 + \cdots)/RT} \\ \beta(V) &= \beta_0 e^{-(a_2 + b_2 V + c_2 V^2 + \cdots)/RT}, \end{aligned} \tag{5.20}$$

where $a_1, a_2, b_1, b_2, c_1, c_2, \ldots$ are constants specific to this transition. It is important to note that in general these parameters are not necessarily interrelated because the three different conformations implicated here (initial, activated, and final, as in figure 5.3) may have very different distributions of charges, resulting in different coefficients in equation (5.17), and thus also resulting in different values for $a_1 \ldots c_2$. In the following discussion, this general functional form for the voltage dependence of rate constants is called the *nonlinear thermodynamic model* (see Destexhe and Huguenard, 2000).

In the "low field limit" (during relatively small transmembrane voltages), the contribution of the higher-order terms may be negligible. Thus, a simple, commonly used voltage dependence results from the first-order approximation of equation (5.20) and takes the form:

$$\begin{aligned} \alpha(V) &= \alpha_0 e^{-(a_1 + b_1 V)/RT} \\ \beta(V) &= \beta_0 e^{-(a_2 + b_2 V)/RT}. \end{aligned} \tag{5.21}$$

In the following discussion, this form with a simple exponential voltage dependence of the rate constants will be called the *linear thermodynamic model.*

A further simplification is to consider that the conformational change consists of the movement of a gating particle with a charge q (Hodgkin and Huxley, 1952; see also Borg-Graham, 1991). The forward and backward rate constants then become

$$\alpha(V) = \alpha_0 e^{-\gamma qFV/RT}$$
$$\beta(V) = \beta_0 e^{(1-\gamma)qFV/RT}, \tag{5.22}$$

where γ is the relative position of the energy barrier in the membrane (between zero and one). The constants α_0 and β_0 can be equated to a fixed constant A by introducing the half-activation voltage V_H, leading to

$$\alpha(V) = Ae^{-\gamma qF(V-V_H)/RT}$$
$$\beta(V) = Ae^{(1-\gamma)qF(V-V_H)/RT}. \tag{5.23}$$

This form was introduced by Borg-Graham (1991) for modeling the gating of ion channels. Its parameters are convenient for fitting experimental data: V_H and q affect the steady-state activation and inactivation curves whereas A and γ only affect the time constant, with no effect on steady-state relations.

The drawback of models in which the rate functions are simple exponentials of voltage is that these functions can reach unrealistically high values, which leads to very small time constants and possibly aberrant behavior. A possible way to solve this problem is to force an artificial saturation of the rate constants (Willms et al., 1999) or impose a minimum value on the time constant (Borg-Graham, 1991).

Another possibility, physically more plausible, is not to limit the approximation of equation (5.20) to linear terms, but include higher-order terms in the voltage dependence of the free energy (Destexhe and Huguenard, 2000). For example, the quadratic expansion of equation (5.20) can be written as

$$\alpha(V) = Ae^{-[b_1(V-V_H)+c_1(V-V_H)^2]/RT}$$
$$\beta(V) = Ae^{[b_2(V-V_H)+c_2(V-V_H)^2]/RT}, \tag{5.24}$$

and similarly, its cubic expansion:

$$\alpha(V) = Ae^{-[b_1(V-V_H)+c_1(V-V_H)^2+d_1(V-V_H)^3]/RT}$$
$$\beta(V) = Ae^{[b_2(V-V_H)+c_2(V-V_H)^2+d_2(V-V_H)^3]/RT}, \tag{5.25}$$

where A, $b_1 \ldots d_2$ are constants as defined earlier.

In addition to the effect of voltage on isolated charges or dipoles, described in equation (5.21), these forms account for more sophisticated effects, such as the deformation of the protein by the electrical field (T. L. Hill and Chen, 1972; Stevens, 1978) or mechanical constraints on charge movement (Destexhe and Huguenard, 2000). It also makes it possible for the model to capture more complicated dependence on voltage than the simple exponential functions of equation (5.21), which may result in more realistic behavior (see section 5.7).

Finally, another way to impose a minimal value on the time constant is to consider that the gate operates via two successive transitions:

$$C_1 \underset{\beta(V)}{\overset{\alpha(V)}{\rightleftarrows}} C_2 \underset{k_2}{\overset{k_1}{\rightleftarrows}} O, \tag{5.26}$$

where C_1 and C_2 are two distinct closed states of the gate. The second transition is not dependent on voltage and therefore acts as a rate-limiting factor when α and β are large compared with k_1 and k_2. In this case, the system will be governed essentially by k_1 and k_2, which therefore impose a limit on the rate of opening and closing of the gate. On the other hand, when α and β are small compared with k_1 and k_2, the system will be dominated by the first transition, while the two states C_2 and O will be in rapid quasi-equilibrium. Although this system apparently solves the problem of having a minimal time constant while still conserving the voltage dependence of the gate, it is nevertheless still unrealistic that the simple exponential representation for α and β permits the first transition to occur arbitrarily fast at some voltages.

Reaction schemes involving multiple states, such as equation (5.26), are reminiscent of another class of models, called Markov models, which are described in more detail in the next section.

5.5 Markov Models

As outlined earlier, the formalism introduced by Hodgkin and Huxley (1952) was remarkably forward looking and closely reproduced the behavior of macroscopic currents. However, Hodgkin-Huxley models are not exact and in fact rest on several approximations, and some of their features are inconsistent with experiments. Measurements on Na^+ channels have shown that activation and inactivation must necessarily be coupled (Armstrong, 1981; Aldrich et al., 1983; Bezanilla, 1985), which is in contrast to the independence of these processes in the Hodgkin-Huxley model. Na^+ channels may also show an inactivation that is not voltage dependent, as in the Hodgkin-Huxley model, but state dependent (Aldrich et al., 1983). Although the latter can be modeled with modified Hodgkin-Huxley kinetics (Marom and Abbott, 1994), these phenomena are best described using Markov models, a formalism more appropriate for describing single channels.

Markov models represent the gating of a channel as occurring through a series of conformational changes of the ion channel protein and assume that the transition probability between conformational states depends only on the present state. The

sequence of conformations involved in this process can be described by state diagrams of the form:

$$S_1 \rightleftarrows S_2 \rightleftarrows \cdots \rightleftarrows S_n, \tag{5.27}$$

where $S_1 \ldots S_n$ represents distinct conformational states of the ion channel. Defining $P(S_i, t)$ as the probability of being in a state S_i at time t and $P(S_i \rightarrow S_j)$ as the transition probability from state S_i to state S_j $(j = 1 \ldots n)$, according to

$$S_i \underset{P(S_j \rightarrow S_i)}{\overset{P(S_i \rightarrow S_j)}{\rightleftharpoons}} S_j, \tag{5.28}$$

leads to the following equation for the time evolution of $P(S_i, t)$:

$$\frac{dP(S_i,t)}{dt} = \sum_{j=1}^{n} P(S_j,t)P(S_j \rightarrow S_i) - \sum_{j=1}^{n} P(S_i,t)P(S_i \rightarrow S_j). \tag{5.29}$$

This equation is called the *master equation* (see e.g., Stevens, 1978; Colquhoun and Hawkes, 1981). The left term represents the "source" contribution of all transitions entering state S_i, and the right term represents the "sink" contribution of all transitions leaving state S_i. In this equation, the time evolution depends only on the present state of the system and is defined entirely by knowledge of the set of transition probabilities (Markovian system). In the limit of large numbers of identical channels, the quantities given in the master equation can be replaced by their macroscopic interpretation. The probability of being in a state S_i becomes the fraction of channels in state S_i, noted s_i, and the transition probabilities from state S_i to state S_j become the rate constants, r_{ij}, of the reactions

$$S_i \underset{r_{ji}}{\overset{r_{ij}}{\rightleftarrows}} S_j. \tag{5.30}$$

In this case, one can rewrite the master equation as

$$\frac{ds_i}{dt} = \sum_{j=1}^{n} s_j r_{ji} - \sum_{j=1}^{n} s_i r_{ij}, \tag{5.31}$$

which is a conventional kinetic equation for the various states of the system. Note that the rate constants can be voltage dependent and can be expressed as earlier (e.g., equation 5.20).

Stochastic Markov models (as in equation 5.29) are adequate to describe the stochastic behavior of ion channels as recorded using single-channel recording techniques (see Sakmann and Neher, 1995). In other cases, where a larger area of

membrane is recorded and large numbers of ion channels are involved, the macroscopic currents are nearly continuous and are more adequately described by conventional kinetic equations, as in equation (5.31) (see Johnston and Wu, 1995). In the following discussion, only systems of the latter type will be considered.

Note that Markov models are more general than the Hodgkin-Huxley formalism and include it as a subclass. Any Hodgkin-Huxley model can be written as a Markov scheme (while the opposite is not true). For example, the Markov model corresponding to the Hodgkin-Huxley sodium channel is (Fitzhugh, 1965):

$$\begin{array}{ccccccc} C_3 & \underset{\beta_m}{\overset{3\alpha_m}{\rightleftharpoons}} & C_2 & \underset{2\beta_m}{\overset{2\alpha_m}{\rightleftharpoons}} & C_1 & \underset{3\beta_m}{\overset{\alpha_m}{\rightleftharpoons}} & O \\ \alpha_h \uparrow\downarrow \beta_h & & \alpha_h \uparrow\downarrow \beta_h & & \alpha_h \uparrow\downarrow \beta_h & & \alpha_h \uparrow\downarrow \beta_h \\ I_3 & \underset{\beta_m}{\overset{3\alpha_m}{\rightleftharpoons}} & I_2 & \underset{2\beta_m}{\overset{2\alpha_m}{\rightleftharpoons}} & I_1 & \underset{3\beta_m}{\overset{\alpha_m}{\rightleftharpoons}} & I. \end{array} \tag{5.32}$$

Here, the different states represent the channel with the inactivation gate in the open state (top) or closed state (bottom) and (from left to right) three, two, one, or none of the activation gates closed. To be equivalent to the m^3 formulation, the rates must have the 3:2:1 ratio in the forward direction and the 1:2:3 ratio in the backward direction. Only the O state is conducting.

The squid delayed rectifier potassium current modeled by Hodgkin and Huxley with four activation gates and no inactivation can be treated analogously (Fitzhugh, 1965; Armstrong 1969), giving

$$C_4 \underset{\beta_m}{\overset{4\alpha_m}{\rightleftharpoons}} C_3 \underset{2\beta_m}{\overset{3\alpha_m}{\rightleftharpoons}} C_2 \underset{3\beta_m}{\overset{2\alpha_m}{\rightleftharpoons}} C_1 \underset{4\beta_m}{\overset{\alpha_m}{\rightleftharpoons}} O. \tag{5.33}$$

5.6 Fitting Models to Experimental Data

We now use some of the formalisms reviewed here and compare them in similar situations. Two situations are considered successively. The first is the voltage-clamp behavior of the sodium channel and the genesis of action potentials, and the second consists of the characteristics of the T-type calcium current and the genesis of bursts of action potentials by the T-current in thalamic neurons.

Models of Na^+ and K^+ Currents Underlying Action Potentials

We compare here the Hodgkin-Huxley model with two Markov models of Na^+ channels. A nine-state Markov model was proposed by Vandenberg and Bezanilla (1991):

$$
\begin{array}{ccccccccccc}
C & \underset{r_6}{\overset{r_5}{\rightleftharpoons}} & C_1 & \underset{r_6}{\overset{r_5}{\rightleftharpoons}} & C_2 & \underset{r_6}{\overset{r_5}{\rightleftharpoons}} & C_3 & \underset{r_2}{\overset{r_1}{\rightleftharpoons}} & C_4 & \underset{r_4}{\overset{r_3}{\rightleftharpoons}} & O \\
 & & & & & & r_{10}\updownarrow r_8 & & & & r_9\updownarrow r_7 \\
 & & & & & & I_1 & \underset{r_3}{\overset{r_4}{\rightleftharpoons}} & I_2 & \underset{r_1}{\overset{r_2}{\rightleftharpoons}} & I_3.
\end{array} \tag{5.34}
$$

This particular nine-state model was selected to fit not only the measurements of macroscopic ionic currents available to Hodgkin and Huxley, but also recordings of single-channel events and measurements of currents resulting directly from the movement of charge during conformational changes of the protein (so-called *gating currents*; see Hille, 2001). The voltage dependence of the transition rates was assumed to be a simple exponential function of voltage (equation 5.21).

To complement the sodium channel model of Vandenberg and Bezanilla, we also examined the six-state scheme for the squid delayed rectifier channel used by Perozo and Bezanilla (1990):

$$
C \underset{r_2}{\overset{r_1}{\rightleftharpoons}} C_1 \underset{r_4}{\overset{r_3}{\rightleftharpoons}} C_2 \underset{r_4}{\overset{r_3}{\rightleftharpoons}} C_3 \underset{r_4}{\overset{r_3}{\rightleftharpoons}} C_4 \underset{r_6}{\overset{r_5}{\rightleftharpoons}} O, \tag{5.35}
$$

where again rates were described by a simple exponential function of voltage (equation 5.21).

The third class of model considered here consists of simplified Markov models of Na^+ and K^+ currents. The model for the Na^+ channel was chosen to have the fewest possible number of states (three) and transitions (four) while still being capable of reproducing the essential behavior of the more complex models. The form of the state diagram was based on a looped three-state scheme in which some transitions were eliminated, giving an irreversible loop (Bush and Sejnowski, 1991; Destexhe et al., 1994):

$$
\begin{array}{ccc}
C & \underset{r_2(V)}{\overset{r_1(V)}{\rightleftharpoons}} & O \\
{\scriptstyle r_4(V)}\nwarrow & & \swarrow{\scriptstyle r_3} \\
 & I. &
\end{array} \tag{5.36}
$$

This model incorporated voltage-dependent opening, closing, and recovery from inactivation, while inactivation was voltage independent. For simplicity, neither opening from the inactivated state nor inactivation from the closed state was permitted. Although there is clear evidence for occurrence of the latter (Horn et al., 1981), it was unnecessary under the conditions of the present simulations. Rate constants were described by

$$
r_i(V) = \frac{a_i}{1 + \exp[-(V - c_i)/b]}, \tag{5.37}
$$

with $c_1 = c_2$ to yield a model consisting of nine total parameters (Destexhe et al., 1994).

The simplified K^+ channel model consisted in a single open or conducting state O, and a single closed state C:

$$
C \underset{r_2(V)}{\overset{r_1(V)}{\rightleftharpoons}} O. \tag{5.38}
$$

Here, the rates $r_1(V)$ and $r_2(V)$ had a sigmoidal voltage dependence similar to that in equation (5.37) (see details in Destexhe et al., 1994).

Na^+ Currents in a Voltage Clamp

The different types of models reviewed here are characterized by different complexity, ranging from a two-state representation (equation 5.38) to transition diagrams involving many states (equation 5.34). The two-state description is adequate for the behavior of some channels (see Labarca et al., 1985; Yamada et al., 1998; Borg-Graham, 1991; Destexhe et al., 1994; Destexhe et al., 1998a), but for most channels more complex models must be considered. To illustrate this, we compared three different models of the fast sodium channel underlying action potentials (figures 5.4 and 5.5).

The responses of the three sodium channel models were compared during a voltage-clamp step from resting potential (−75 mV) to a depolarized level of −20 mV (figure 5.4). For all three models, the closed states were favored at hyperpolarized potentials. Upon depolarization, forward (opening) rates sharply increased whereas closing (backward) rates decreased, causing a migration of channels in the forward direction toward the open state. The three closed states in the Hodgkin-Huxley model and the five closed states in the Vandenberg-Bezanilla model gave rise to the characteristic delayed activation and sigmoidal shape of the rising phase of the sodium current (figure 5.4d). In contrast, the simple model, with a single closed state, produced a first-order exponential response to the voltage step and was therefore not sigmoidal.

These models generate different predictions about single-channel behavior. The steady-state behavior of the Hodgkin-Huxley model of the macroscopic sodium current is remarkably similar to that of the Vandenberg-Bezanilla (1991) model, but there are important differences in the relationship between activation and inactivation. First, as mentioned earlier, in the Hodgkin-Huxley model, activation and inactivation are kinetically independent. This independence has been shown to be untenable on the basis of gating and ion current measurements in the squid giant

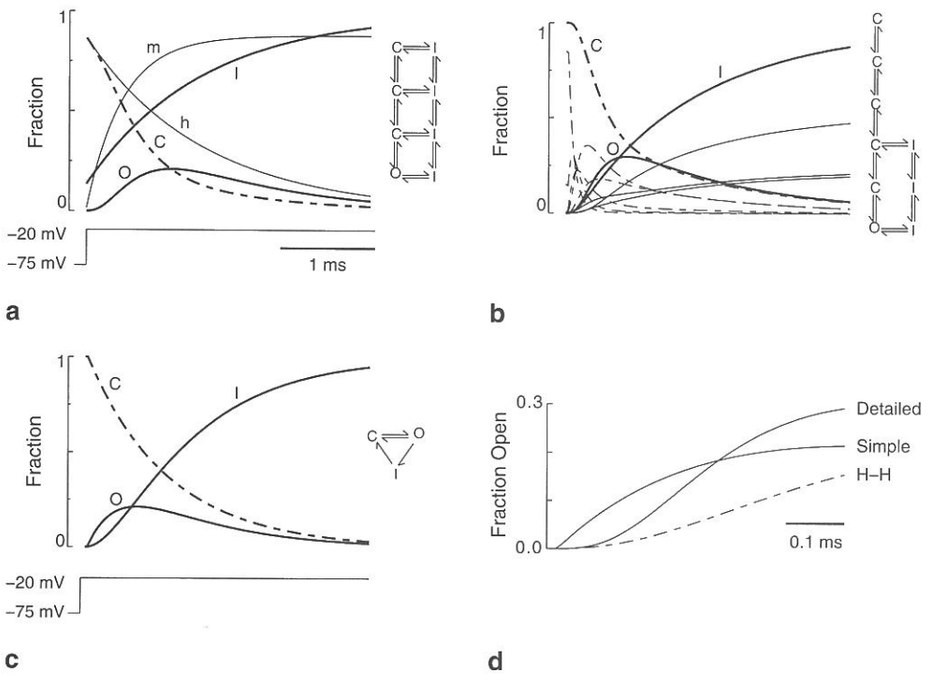

Figure 5.4
Three kinetic models of a squid axon sodium channel produce qualitatively similar conductance time courses. A voltage-clamp step from rest, $V = -75$ mV, to $V = -20$ mV was simulated. The fraction of channels in the open state (O, thick solid line), closed states (C, thick dashed lines), and inactivated states (I, thick dotted lines) are shown for the Hodgkin-Huxley model (1952), a detailed Markov model (Vandenberg and Bezanilla, 1991), and a simple Markov model (Destexhe et al., 1994). (a) Hodgkin-Huxley model of the sodium channel (equation 5.32). The activation (m) and inactivation (h) gates were deduced from other states and are indicated by thin lines. (b) Markov model of Vandenberg and Bezanilla (1991; equation 5.34). Individual closed and inactivated states are shown (thin lines), as well as the sum of all five closed states (C), the sum of all three inactivated states (I) and the open state (O). (c) Simplified three-state Markov model (Destexhe et al., 1994; equation 5.36). (d) Comparison of the time course of open channels for the three models on a faster time scale shows differences immediately following the voltage step. The Hodgkin-Huxley (H-H) and Vandenberg-Bezanilla (detailed) models give smooth, multiexponentially rising phases, while the three-state Markov model (simple) gives a single exponential rise with a discontinuity in the slope at the beginning of the pulse. (Figure modified from Destexhe et al., 1994, where all details are given.)

axon (Armstrong, 1981; Aldrich et al., 1983; Bezanilla, 1985). Consequently, Markov models that reproduce gating currents, such as the Vandenberg-Bezanilla model examined here, require schemes with coupled activation and inactivation. Likewise, in the simple model, activation and inactivation were strongly coupled, owing to the unidirectional looped scheme (equation 5.36), so that channels were required to open before inactivating and could not reopen from the inactivated state before closing.

A second difference is that in the Hodgkin-Huxley and Vandenberg-Bezanilla models, inactivation rates are slow and activation rates are fast. In the simplified Markov model, the situation was reversed, with fast inactivation and slow activation. At the macroscopic level modeled here, these two relationships gave rise to similar time courses for open channels (figure 5.4a–c; see Andersen and Koeppe, 1992). However, the two classes of models make distinct predictions for single-channel behavior. Whereas the Hodgkin-Huxley and Vandenberg-Bezanilla models predict the latency to the first channel opening to be short and channel open times to be comparable to the time course of the macroscopic current, the simplified Markov model predicts a large portion of first channel openings to occur after the peak of the macroscopic current and to have open times much shorter than the current's duration.

Genesis of Action Potentials (Current Clamp)

Despite significant differences in their complexity and formulation, the three models of the sodium channel all produced comparable action potentials and repetitive firing when combined with appropriate delayed-rectifier potassium channel models (figure 5.5). These simulations thus seem to perform similarly for fitting the macroscopic behavior of Na^+ and K^+ currents.

However, these three models generated clear differences when compared in a voltage clamp (figure 5.4) and still larger differences would be expected at the single-channel level. Thus, the choice of model clearly depends on the scope of the modeling study. If the detailed behavior of voltage-clamp experiments or single-channel recordings is to be reproduced, Markov models are certainly the most appropriate representation. However, if the goal is to reproduce the qualitative features of membrane excitability, action potentials, and repetitive firing, all models seem equivalent, except that simpler models are faster to compute. Thus in this case, simplified two- or three-state schemes or the Hodgkin-Huxley model would seem most appropriate.

5.7 Models of the T-Type Calcium Current

The different formalisms reviewed earlier are now applied to the example of voltage-clamp experiments of the T-type (low threshold) calcium current responsible for bursting behavior in thalamic neurons (Jahnsen and Llinás, 1984).

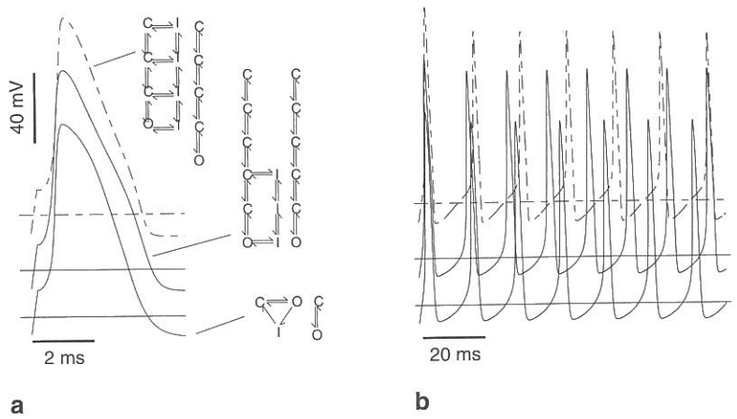

Figure 5.5
Similar action potentials produced using three different kinetic models of squid fast sodium and delayed rectifying potassium channels. (a) Single action potentials in response to 0.2-ms, 2-nA current pulse are elicited at similar thresholds and produce similar waveforms using three different pairs of kinetic models: Hodgkin and Huxley (1952) (dot-dashed line), detailed Markov models (Perozo and Bezanilla, 1990; Vandenberg and Bezanilla, 1991) (dotted line), and simplified kinetic models (solid line). (b) Repetitive trains of action potentials elicited in response to sustained current injection (0.2 nA) have slightly different frequencies. Sodium channels were modeled as described in figure 5.4. The detailed Markov potassium channel model had six states (Perozo and Bezanilla, 1990; equation 5.35) and the simple model of potassium channel had two states (equation 5.38). (Figure modified from Destexhe et al., 1994, where all details are given.)

Hodgkin-Huxley Model of the T-Current

The voltage-clamp behavior shown here was first modeled by a Hodgkin-Huxley type of representation in which rate constants were fit to experimental data using empirical functions of voltage (Huguenard and McCormick, 1992). Owing to the nonlinear behavior of calcium currents (the internal and external Ca^{2+} concentrations differ by about four orders of magnitude), they were represented using the constant-field equation (equation 5.12). The variables m and h in this equation represent, respectively, the activation and inactivation variables and obey first-order equations similar to equation (5.8). Their steady-state relations were fit using Boltzmann equations (figure 5.6a–b, thin solid lines), leading to the following optimal functions:

$$m_\infty(V) = 1/(1 + \exp[-(V + 57)/6.2]) \tag{5.39}$$

$$h_\infty(V) = 1/(1 + \exp[(V + 81)/4]). \tag{5.40}$$

Similarly, the voltage-dependent time constants were estimated by fitting exponential functions to the values determined experimentally (figure 5.6c–d, thin solid lines), leading to the following expression for activation:

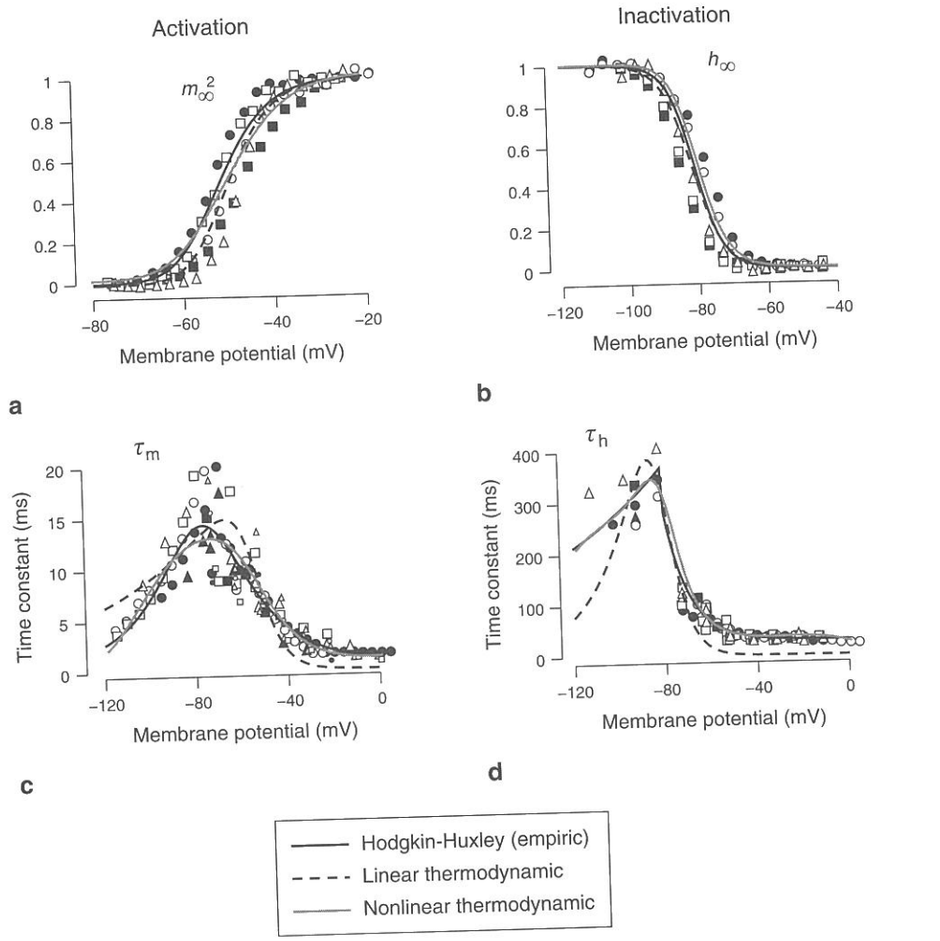

Figure 5.6
Fitting of different models to the T-current in thalamic relay neurons. In each panel, the symbols show the voltage-clamp data obtained in several thalamic neurons (see figures 5.1 and 5.2) and the continuous curves show the best fits obtained with an empirical Hodgkin-Huxley-type model (thin solid line), a linear thermodynamic model (dashed line), and a nonlinear thermodynamic model (thick solid line). (a) Steady-state activation (m_∞^2). (b) Steady-state inactivation (h_∞). (c) Activation time constant (τ_m). (d) Inactivation time constant (τ_h). The leftmost symbols in d (≤ -80 mV) are the data from the slow recovery from inactivation of the T-current. See the text for the values of the parameters. All functions were fit using a simplex method. (Figure modified from Destexhe and Huguenard, 2000.)

$$\tau_m(V) = 0.612 + 1/(\exp[-(V + 132)/16.7] + \exp[(V + 16.8)/18.2]) \tag{5.41}$$

and for inactivation:

$$\tau_h(V) = 28 + \exp[-(V + 22)/10.5] \quad \text{for } V >= -81 \text{ mV}$$
$$\exp[(V + 467)/66.6] \quad \text{for } V < -81 \text{ mV}. \tag{5.42}$$

Here two different functions were fit to the time constants τ_h obtained from inactivation protocols ($V >= -81$) or recovery from inactivation ($V < -81$).

The temperature dependence of these empirical functions was adjusted according to the following rule:

$$\tau' = \tau Q_{10}^{-(T-24)/10}, \tag{5.43}$$

where Q_{10} is the experimentally determined change of time constants for a 10-degree difference in temperature. For the T-current in thalamic neurons, Q_{10} was determined as equal to 5 for τ_m and 3 for τ_h (Coulter et al., 1989).

The behavior of this model is shown in figure 5.7a. The model accounted well for all protocols of figures 5.1 and 5.2, with activation and recovery from inactivation shown in figures 5.7a1 and a2, respectively. However, in this model, τ_m and τ_h were fit using functions of voltage obtained empirically. Similar to the work of Hodgkin and Huxley (1952), this approach leads to a model that accounts well for the current-clamp behavior of the T-current in thalamic neurons (McCormick and Huguenard, 1992; see figure 5.8).

Linear Thermodynamic Model of the T-Current

Another possibility is to deduce the functional form of rate constants from thermodynamic arguments. The first of such models is the linear approximation. Constraining the fitting using rate constants described by equation (5.21) (figure 5.6, dashed lines) led to the following optimal expressions:

$$\alpha_m = 0.049 \exp[444\gamma_m(V + 54.6)/RT] \tag{5.44}$$

$$\beta_m = 0.049 \exp[-444(1 - \gamma_m)(V + 54.6)/RT] \tag{5.45}$$

$$\alpha_h = 0.00148 \exp[-559\gamma_h(V + 81.9)/RT] \tag{5.46}$$

$$\beta_h = 0.00148 \exp[559(1 - \gamma_h)(V + 81.9)/RT], \tag{5.47}$$

where $\gamma_m = 0.90$ and $\gamma_h = 0.25$. The steady-state relations and time constants are obtained similarly to those in equations (5.9–5.10).

This model provided a good fit of the steady-state relations (figure 5.6a–b, dashed lines), but the fit to time constants was poor (figure 5.6c–d, dashed lines). In particular,

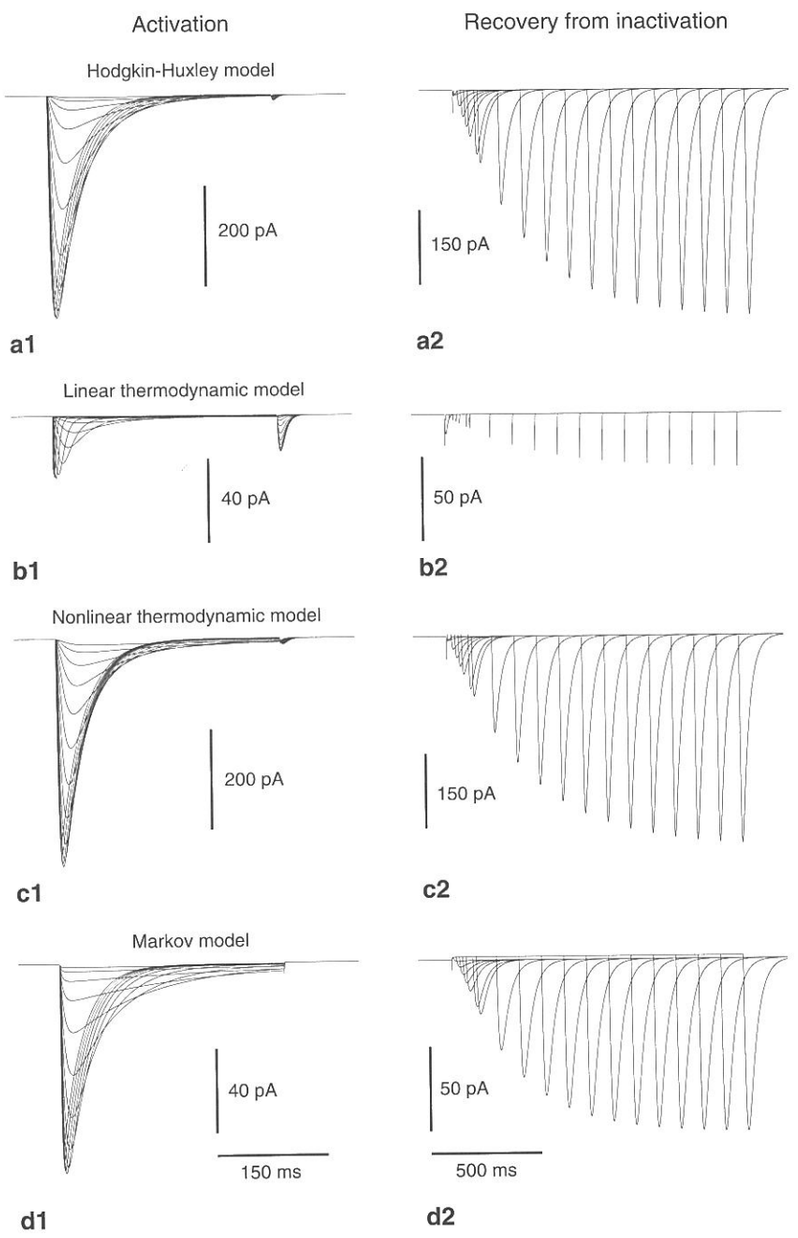

Figure 5.7
Voltage-clamp behavior of different models of the T-current. Left panels: activation protocol (identical to figure 5.1a2); right panels: protocol for the recovery from inactivation (identical to figure 5.2a2). (a) Empirical Hodgkin-Huxley-type model. (b) Linear thermodynamic model. (c) Nonlinear thermodynamic model. (d) Markov model. In all cases, the same density of T-channels was used ($\bar{P}_{Ca} = 3 \times 10^{-6}$ cm/s. (Figure modified from Destexhe and Huguenard, 2000.)

it was not possible to capture the saturation of τ_m and τ_h to constant values for depolarized membrane potentials. This poor fit had catastrophic consequences, as illustrated in figure 5.7b. Owing to the near-zero time constants at depolarized levels, the current activated and inactivated too fast and led to peak current amplitudes that were more than an order of magnitude smaller than the Hodgkin-Huxley model at the same channel densities (compare a and b in figure 5.7). We conclude that linear thermodynamic models do not provide an acceptable behavior in a voltage clamp for the T-current.

One possibility of resolving this inherent limitation is to add an artificial minimum value to the time constant (Borg-Graham, 1991), but this possibility was not considered here in order to stay within a physically plausible formalism. Instead, we show next that this problem can be solved by including higher-order voltage-dependent contributions in the free-energy barrier (Destexhe and Huguenard, 2000).

Nonlinear Thermodynamic Model of the T-Current

Nonlinear thermodynamic models assume that the free-energy barrier depends nonlinearly on voltage (see equation 5.20) and that each conformational state involved has its own dependence on voltage, independently of other conformational states (Destexhe and Huguenard, 2000). The consequence is that the coefficients $a_1 \ldots c_2$ in equation (5.20) can take any value independently of each other. Using these nonlinear expressions to fit the voltage-clamp data of the T-current led to better fits of T-channel data. The quadratic expansion still provided a poor fit of the time constants, although better than linear fits (not shown). Acceptable fits were obtained for a cubic expansion of the rate constants, given by

$$\begin{aligned}
\alpha_m(V) &= A_m \exp[b_{m1}(V - V_m) + c_{m1}(V - V_m)^2 + d_{m1}(V - V_m)^3]/RT \\
\beta_m(V) &= A_m \exp[b_{m2}(V - V_m) + c_{m2}(V - V_m)^2 + d_{m2}(V - V_m)^3]/RT \\
\alpha_h(V) &= A_h \exp{-}[b_{h1}(V - V_h) + c_{h1}(V - V_h)^2 + d_{h1}(V - V_h)^3]/RT \\
\beta_h(V) &= A_h \exp[b_{h2}(V - V_h) + c_{h2}(V - V_h)^2 + d_{h2}(V - V_h)^3]/RT.
\end{aligned} \tag{5.48}$$

The best fit of this nonlinear thermodynamic model is shown in figure 5.6 (thick solid lines) and was obtained with the following parameters: $A_m = 0.053$ ms^{-1}, $V_m = -56$ mV, $b_{m1} = -260$, $c_{m1} = 2.20$, $d_{m1} = 0.0052$, $b_{m2} = 64.85$, $c_{m2} = 2.02$, $d_{m2} = 0.036$, $A_h = 0.0017$ ms^{-1}, $V_h = -80$ mV, $b_{h1} = 163$, $c_{h1} = 4.96$, $d_{h1} = 0.062$, $b_{h2} = -438$, $c_{h2} = 8.73$, $d_{h2} = -0.057$. Figure 5.6 (thick solid lines) shows that this model could capture the form of the voltage dependence of the time constants. In particular, it

could fit the saturating values for the time constants at a depolarized level in a manner similar to the empirical functions used for the Hodgkin-Huxley-type model (figure 5.6, thin solid lines). Nonlinear expansions of higher order provided better fits, but the difference was not qualitative (not shown).

Using these rate constants with equation (5.39) produced acceptable voltage-clamp behavior, as shown in figure 5.7c. All protocols of activation (figure 5.7c1), deactivation (not shown), inactivation (not shown), and recovery from inactivation (figure 5.7c2) showed voltage-dependent behavior similar to that of the experimental data.

Markov Model of the T-Current

To illustrate the Markov representation, we have used a model of the T-current introduced by Chen and Hess (1990). This model was obtained based on voltage-clamp recordings and single-channel recordings of the T-current in fibroblasts, and the following optimal scheme was proposed (Chen and Hess, 1990):

$$\begin{array}{ccccc}
C_1 & \underset{k_d(V)}{\overset{k_a(V)}{\rightleftharpoons}} & C_2 & \underset{k_c}{\overset{k_o}{\rightleftharpoons}} & O \\
{\scriptstyle k_{-r}}\uparrow\downarrow{\scriptstyle k_r} & & & & {\scriptstyle k_i}\uparrow\downarrow{\scriptstyle k_{-i}} \\
I_1 & \underset{k_b(V)}{\overset{k_f(V)}{\rightleftharpoons}} & & & I_2
\end{array} \tag{5.49}$$

Here, only k_a, k_d, k_f, and k_b are voltage dependent, while the other rates are constant. Thus activation occurs through one voltage-dependent step (k_a, k_d) and one voltage-independent step (k_o, k_c), the latter being rate limiting if k_a and k_d reach high values. Similarly, the inactivation occurs first through a voltage-independent step (k_i, k_{-i}), followed by a voltage-dependent transition (k_f, k_b) and a voltage-independent return to the closed state (k_r, k_{-r}).

Fitting the parameters of Markov models to experimental data is in general difficult (Cannon and D'Alessandro, 2006). It is not possible to obtain an analytical expression for both time constants and steady-state relations, owing to the too-great complexity of the model. In general, the activation and inactivation will be described by multiexponential processes with several time constants, and relating these multiple time constants to the time constants estimated from experimental data (figures 5.1–5.2) is not trivial. Rather, the parameters of Markov models are deduced from various experimental considerations. It is also possible to directly fit the Markov model to the original voltage-clamp traces by minimizing the error between the model and all experimental traces. Although in principle more accurate, this procedure is difficult to realize in practice because of the complexity of the model (eleven parameters here).

The choice of these parameters was guided by the following considerations (Chen and Hess, 1990): (1) The value of k_i must be close to the saturating value of the rate of inactivation at depolarized membrane potentials (figure 5.2c), and k_{-i} must be much smaller to ensure complete inactivation. (2) k_c must be close to the fastest activation time constants at negative potentials (figure 5.1c), while k_o must be large (>1 ms^{-1}) to be compatible with the short bursts of opening in single-channel recordings (Chen and Hess, 1990). (3) The sum $k_r + k_{-r}$ determines the rate of recovery from inactivation at negative membrane potentials. (4) The values of k_a and k_d are adjusted to obtain the best fit with activation and inactivation voltage-clamp recordings using a thermodynamic template with a linear dependence of the free energy on voltage:

$$k = k_0 \exp(qFV/RT), \tag{5.50}$$

where $q = 3.035$ is the net charge of a gating particle.

Since this scheme is cyclic, microscopic reversibility requires that the clockwise product of the rate constants equal the anticlockwise product, which in turn requires that the voltage dependence of k_f and k_b be the same as that of k_a and k_d. The optimal values of the rate constants were (all units are ms^{-1}):

$$\begin{aligned}
k_a &= 6.4 \exp[qF(V-s)/RT] \\
k_d &= 0.000502 \exp[-qF(V-s)/RT] \\
k_f &= 16 \exp[qF(V-s)/RT] \\
k_b &= 2 \times 10^{-6} \exp[-qF(V-s)/RT] \\
k_o &= 3 \\
k_c &= 0.7 \\
k_i &= 0.036 \\
k_{-i} &= 8 \times 10^{-5} \\
k_r &= 0.001 \\
k_{-r} &= 0.003.
\end{aligned} \tag{5.51}$$

Here, the parameters were adapted to recordings of the T-current in thalamic neurons. An additional parameter, $s = -5$ mV, was introduced to shift the voltage dependence to adjust the model to the thalamic T-current.

This model was simulated with the above expressions for rate constants and the T-current described by the following equation:

$$I_T = \bar{P}_{Ca}[O]G(V, Ca_o, Ca_i), \tag{5.52}$$

where $[O]$ is the fraction of channels in the open state. Simulated voltage-clamp experiments (figure 5.7d) show that the Chen and Hess model reproduced well the activation characteristics of the T-current (figure 5.7d1) as well as its slow recovery from inactivation (figure 5.7d2). However, this model did not quantitatively fit the T-current of thalamic neurons because it was based on single-channel recordings of the T-current in fibroblasts, which is different than the "neuronal" T-current (see analysis in Chen and Hess, 1990; see also Cannon and D'Alessandro, 2006). Obtaining a better Markov representation of the thalamic T-current would require constraining the model by single-channel recordings.

Comparison of the Different Models (Current Clamp)

The different models reviewed here for the T-current were compared in a current clamp. A single-compartment model of the thalamic relay neuron was generated (same parameters as in Destexhe et al., 1998b) and contained leak currents and the T-current according to the following equation:

$$c_m \frac{dV}{dt} = -g_L(V - E_L) - I_T, \tag{5.53}$$

where $c_m = 0.88$ $\mu F/cm^2$ is the membrane capacitance, $g_L = 0.038$ mS/cm^2 and $E_L = -77$ mV are the leak conductance and reversal potential, and I_T is the T-current as given by equation (5.12). These parameters were obtained by matching the model to thalamic neurons recorded in vitro (Destexhe et al., 1998b).

Using this model, the genesis of low-threshold spikes (LTSs) was monitored through return to resting potential after injection of hyperpolarizing currents. The empirical Hodgkin-Huxley-type model of the T-current generated LTSs in a grossly all-or-none fashion (figure 5.8a). The linear thermodynamic model (figure 5.8b) did not generate LTSs, which is consistent with the very small amplitude of the current evidenced earlier (figure 5.7b). On the other hand, the nonlinear thermodynamic model (figure 5.8c) and the Markov model of the T-current (figure 5.8d) presented a behavior more consistent with the Hodgkin-Huxley-type model. The peak amplitude of the LTSs was compared using different models in figure 5.8e. Although the shapes of the LTSs were not identical, Hodgkin-Huxley and nonlinear thermodynamic models produced remarkably similar peak amplitudes (filled circles and triangles in figure 5.8e). We therefore conclude that nonlinear thermodynamic models provide fits of a quality comparable to empirical Hodgkin-Huxley models, but that their form is physically more plausible.

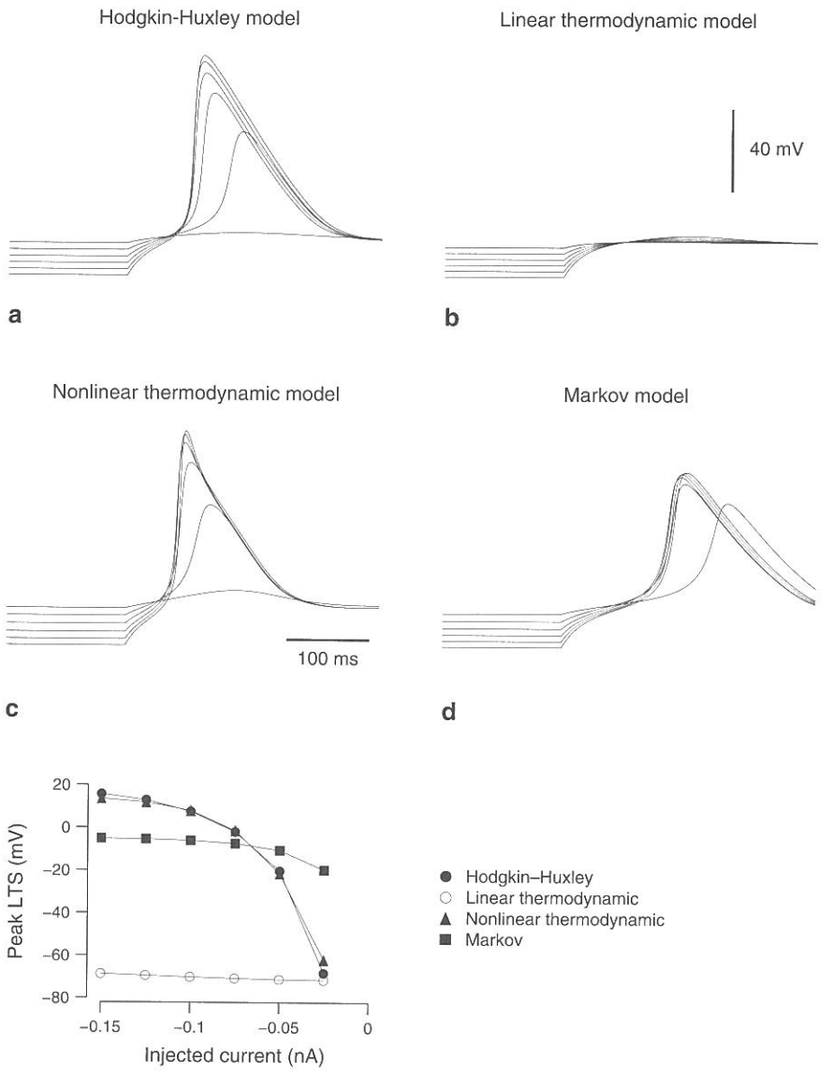

Figure 5.8
Low-threshold spikes generated by different models of the T-current. Comparison of the same current-clamp simulation for four different models of the T-current: an empirical Hodgkin-Huxley-type model (a), a linear thermodynamic model (b), a nonlinear thermodynamic model (c), and a Markov model (d). The simulation consisted in injecting hyperpolarizing current pulses of various amplitudes (−0.025, −0.05, −0.075, −0.1, −0.125, and −0.15 nA) and of 1 s duration. At the end of the pulse, the model generated a low-threshold spike (LTS) upon return to rest. (e) Peak amplitude of low-threshold spikes generated by the different models of the T-current. All simulations were done with the same single-compartment geometry, which contained leak currents in addition to the T-current (identical parameters as in Destexhe et al., 1998). The density of T-channels was identical in all cases ($\bar{P}_{Ca} = 5 \times 10^{-5}$ cm/s) and was in the range of densities estimated from rat ventrobasal thalamic neurons (Destexhe et al., 1998a). (Figure modified from Destexhe and Huguenard, 2000.)

5.8 Conclusions

In this chapter, using concrete examples, we have illustrated several widely used formalisms to model voltage-dependent channels, and discussed how to fit the corresponding equations and parameters to experimental data (for a recent review, see Cannon and D'Alessandro, 2006).

The question of which formalism to choose for modeling voltage-dependent channels is of course entirely dependent on the type of data available and the goal of the modeling effort (see also discussion in Bruno et al., 2005). It is clear that a two-state scheme cannot capture the features of single-channel recordings, which require Markov models of sufficient complexity to account for the data. On the other hand, even simplified two- or three-state representations can capture phenomena such as action potentials (Destexhe et al., 1994). For example, if the principal requirement is to generate action potentials, it is not necessary to include all the complexity of the most sophisticated Markov diagrams of channels, and simplified representations appear sufficient. This simplistic approach may be adequate for models involving large-scale networks of thousands of cells, for which computational efficiency is a more important concern than reproducing all the microscopic features of the channels.

Finally, we would like to point to a number of resources available for modeling ion channels. The first type consists of databases freely available on the Internet. The most prominent of modeling databases is the ModelDB database (http://senselab.med.yale.edu/senselab/ModelDB), which provides a considerable number of program codes of published models, written using many different publically available simulation environments. The ChannelDB database (http://www.genesis-sim.org/hbp/channeldb/ChannelDB.html) provides the user with a large number of ion channel models stored in simulator-independent NeuroML format. The NeuronDB database (http://senselab.med.yale.edu/senselab/NeuronDB) also contains useful information about the gating properties of different types of ion channels. A second type of resource is dedicated software for fitting ion channel models from experimental data. Some simulation environments, such as NEURON (see the software appendix), include automated procedures to perform such a fitting. There exist also toolboxes and free packages for fitting ion channel models to experimental data, such as NEUROFIT (http://www.uoguelph.ca/~awillms/neurofit/) for Hodgkin-Huxley models, or QuB (http://www.qub.buffalo.edu/) for Markov models. These resources are growing fast, which underlines the need for centralizing all resources in a unified database for all computational neuroscience research.